Appl. Phys. A 79, 761–765 (2004)
DOI: 10.1007/s00339-004-2652-8

Applied Physics A
Materials Science & Processing

C. CHENG
X. XU✉

Molecular dynamic study of volumetric phase change induced by a femtosecond laser pulse

School of Mechanical Engineering, Purdue University, West Lafayette, IN 47907, USA

Received: 26 September 2003/Accepted: 4 February 2004
Published online: 26 July 2004 •

ABSTRACT During the last decade, femtosecond laser has been used for micro-machining of various materials. In this work, the phase change phenomena during femtosecond laser ablation are investigated using molecular dynamics (MD) simulation. The process of femtosecond laser ablation of nickel is calculated. The temperature and stress history, and the generation and growth of gas bubbles are traced. For different laser pulse fluences, the material ablation process is analysed to reveal the effect of temperature and stress.

PACS 02.70.Ns; 42.62.-b; 64.60.Ht

1 Introduction

Laser ablation is the process of the material removal after laser is irradiated on the target surface. It has been used as an important tool for material processing and structuring in many technological areas. Over the last decade, it has been shown that femtosecond lasers have particular advantages in material processing, such as highly localized material removal and reduced heat-affected zone compared with nanosecond laser processing [1–3]. However, little is conclusive about the microscopic mechanism leading to laser ablation. Normal experimental instruments cannot capture the ablation phenomenon precisely, which usually happens at the timescale of the order of picosecond or less, and is confined in a spatial scale of nanometres in the direction of laser irradiation. Also, the macroscopic heat transfer and fluid mechanics equations obtained under the continuum assumption are of doubt since femtosecond laser ablation is a highly non-equilibrium process.

During recent years, molecular dynamics (MD) has demonstrated its potential for studying the laser ablation mechanism, especially for femtosecond laser ablation [4–6]. MD tracks the motion of each molecule or atom at every time step, so the detailed ablation phenomenon is traced and recorded. MD calculations do not need macroscopic material properties as a priori. The only equation for the molecules (or atoms) is the Newtonian motion equation determined by the intermolecular (or inter-atomic) potential, which governs the motion of the molecules (or atoms). Therefore, MD has particular advantages in handling non-equilibrium energy transfer at the micro and nano-scale, including laser ablation of a thin layer of material. In this work, molecular dynamics simulation is used to investigate laser ablation of nickel. Proper techniques for dealing with the pressure boundary condition and for calculation of stress waves are applied. Our main goal is to illustrate the process of material removal during femtosecond laser ablation in detail, and to discuss the mechanism of the ablation process.

✉ E-mail: xxu@ecn.purdue.edu

2 Simulation method

The problem considered in this work deals with a femtosecond laser pulse radiating perpendicularly onto a nickel target in vacuum whose initial temperature is 300 K. The computational domain has a thickness (in the x direction) of 186.5 nm. It is assumed that the target is infinitely large in the lateral direction, so periodical boundary conditions are applied in the y and z directions. The calculation domain has the lateral dimension of 10.6×10.6 nm. The laser pulse has a uniform spatial distribution and a temporal Gaussian distribution of 100 fs FWHM centred at $t = 1$ ps. The laser energy is absorbed exponentially into the target, with an absorption depth of 8 nm [7]. The laser fluence absorbed by the target ranges from $0.25\,\mathrm{J/cm^2}$ to $1.0\,\mathrm{J/cm^2}$.

The process of the MD simulation used in this work is briefly described as follows. First, the initial positions of atoms are determined according to the FCC lattice structure of the nickel crystal. The initial velocities are randomly distributed, and the Maxwell-Boltzmann distribution, the equilibrium velocity distribution, is established after several hundreds of time steps [8]. For each time step, the force acting on each atom is calculated from the Morse pair potential function as

$$\Phi(r) = D\left[\mathrm{e}^{-2b(r-r_\varepsilon)} - 2\,\mathrm{e}^{-b(r-r_\varepsilon)}\right] \quad (1)$$

where D is the total dissociation energy and r_ε is the equilibrium distance evaluated as 0.4205 eV and 0.278 nm for nickel, respectively. The constant b in this equation determines the shape of the potential curve, with a value of $14.199\,\mathrm{nm^{-1}}$ [9]. A cut-off distance is used, beyond which the force between two atoms is neglected. To organize the force evaluation considering the cut-off distance, the cell structure and linked list method is used [8]. Computations of the velocity and position follow the modified Verlet algorithm [10].

Periodical boundary conditions are used along the y and z directions. The surface irradiated by the laser pulse is subject to the free boundary condition. At the bottom of the target, the so-called "non-reflecting pressure boundary condition" is applied. This method was first introduced by Schäfer et al. [11], and its use in computing laser ablation has been described in detail in [12].

In this simulation, the two-temperature model [13] is applied to calculate laser heating of electrons. Laser energy is absorbed by electrons only, and is then transferred to the lattice. The governing equation for the electron system is

$$C_{\mathrm{e}}\frac{\partial T_{\mathrm{e}}}{\partial t}=\frac{\partial}{\partial x}\left(\kappa_{\mathrm{e}}\frac{\partial T_{\mathrm{e}}}{\partial x}\right)-G\left(T_{\mathrm{e}}-T_{\mathrm{l}}\right)+S \tag{2}$$

where T_{e} and T_{l} are the temperatures of electrons and the lattice, respectively. C_{e} is the volumetric specific heat calculated as $C_{\mathrm{e}}\left(T_{\mathrm{e}}\right)=\gamma T_{\mathrm{e}}$, and $\gamma=1.065\times10^{3}\,\mathrm{J/m^{3}\text{-}K^{2}}$. The temperature dependence of the thermal conductivity of electrons k_{e} is approximated as $\kappa_{\mathrm{e}}=\kappa_{\mathrm{e},0}T_{\mathrm{e}}/T_{\mathrm{l}}$, and $\kappa_{e,0}=91\,\mathrm{W/m\text{-}K}$ [14]. $G(T_{\mathrm{e}}-T_{\mathrm{l}})$ is the electron-lattice coupling term. The value of G is taken as $3.6\times10^{17}\,\mathrm{W/m^{3}\text{-}K}$ [15]. S is the laser heating source term. Equation (2) is solved using the tri-diagonal matrix algorithm (TDMA) method.

After being irradiated by the laser pulse, the surface of the target expands or even separates from the bulk. This will affect the energy dissipation inside the material. This effect is considered in the following way. The thermal conductivity and specific heat of electrons in each cell are scaled with the density change. Therefore, when expansion happens, the effective thermal conductivity and specific heat decrease, which is consistent with the electron properties for metals [16].

Transfer of laser energy to the lattice is simulated by scaling the velocities of all atoms by a factor $\sqrt{1+\frac{G(T_{\mathrm{e}}-T_{\mathrm{l}})\Delta t}{E_{k,t}}}$, where $E_{k,t}$ is the kinetic energy at the time step t. The lattice conduction is always considered in the MD simulation, although it is small compared with the electron conduction in a metal.

Stress is another important quantity for the investigation of laser ablation. In this simulation, stress along the laser propagation direction is evaluated as [17]

$$\sigma_{xx}=-\varrho k_{b}T-\frac{1}{V}\left\langle\sum_{i=1}^{N}\sum_{i<j}F_{ij}x_{ij}\right\rangle \tag{3}$$

where F_{ij} and x_{ij} are the x direction components of the force and distance between two atoms, respectively.

In order to capture the laser ablation process, a large number of atoms are computed. The total number of atoms is about 1 900 000 and parallel processing technique is applied to accelerate the computation. A cluster composed of eight 2.0 GHz PCs is used, and MPICH, a potable implementation of message-passing interface, the standard for message-passing libraries, is applied for the parallel MD calculation. The overall efficiency of the parallel program is about $90\sim92\%$ on eight nodes. More descriptions of the parallel calculation can be found in [12].

3 Results and discussion

The main goal of this simulation is to study the mechanism of femtosecond laser ablation. Therefore, the results presented here are chosen at certain time steps to show the detailed process of laser ablation.

Figure 1 shows snapshots of part of the calculation domain at laser fluences of $0.25\,\mathrm{J/cm^{2}}$, $0.285\,\mathrm{J/cm^{2}}$, $0.65\,\mathrm{J/cm^{2}}$ and $1.0\,\mathrm{J/cm^{2}}$. Each atom is represented by a dot. To observe the interior of the target, the whole domain is sliced into 10 layers with identical thickness in the y direction, and the 5th layer is shown in these figures except Fig. 1e, where the whole thickness is displayed. Only the near surface region where the laser energy is absorbed and laser ablation occurs is shown in the figure.

From Fig. 1, it is seen that no gas bubbles are generated for the laser fluence of $0.25\,\mathrm{J/cm^{2}}$, although evaporation is seen at the surface. For the laser fluences at 0.285, 0.65 and $1.0\,\mathrm{J/cm^{2}}$, gas bubbles are generated inside the domain, and grow larger at later time steps. It is also seen that the average size and the number of the bubbles are strongly dependent on the laser fluence. At $0.285\,\mathrm{J/cm^{2}}$, only several bubbles appear, and the size grows much larger at later time steps. However, for $0.65\,\mathrm{J/cm^{2}}$ and $1.0\,\mathrm{J/cm^{2}}$, the number of bubbles is much larger, while the average size of the bubbles is much smaller. The dependence of the bubble size on the laser fluence qualitatively agrees with the kinetic theory of nucleation. Our calculation finds that the maximum temperature increases with increasing laser fluence. At a higher temperature, the energy needed for vapour embryos to grow to nuclei, as well as the size of the nuclei, decreases. (Embryos smaller than a critical size will collapse, while those larger than the critical radius, called nuclei, will favour growing in order to reduce free energy.) Therefore, a decrease of the bubble size with increasing laser fluence is expected. It is seen from Fig. 1d and e that liquid droplets form at the surface region for laser fluence at $1.0\,\mathrm{J/cm^{2}}$ after 57 ps. This is similar to the results shown in [18]. However, no clear dependence for the size of the droplets on the location is seen, which is different from the results in [18]. This discrepancy could be attributed to the different potential function, material properties, or laser duration/fluences used.

To reveal the detailed process of bubble generation and growth, the lattice temperature and stress wave at the laser fluence of $0.285\,\mathrm{J/cm^{2}}$ at different time steps are shown in Fig. 2. At time 0, the target is at an equilibrium state of 300 K. The stress is almost zero. After the laser pulse is incident on the target, the surface temperature increases dramatically, and a strong compressive stress is generated on the surface and perpetrates into the target. A positive stress, which represents a tensile stress wave, follows the compressive wave, but its magnitude is much smaller. Melting occurs at the surface at about 6 ps (which is not shown in the figure). It is also noticed that the temperature of the solid–liquid interface is about 3800 K, much higher than the melting temperature of nickel, indicating the existence of strong over-heating. This interfacial temperature decreases at later time steps and reaches about 2750 K at 90 ps, and the melting process slows down but has not stopped. It needs to be pointed out that the calculated melting temperature is 2500 ± 100 K, different from the

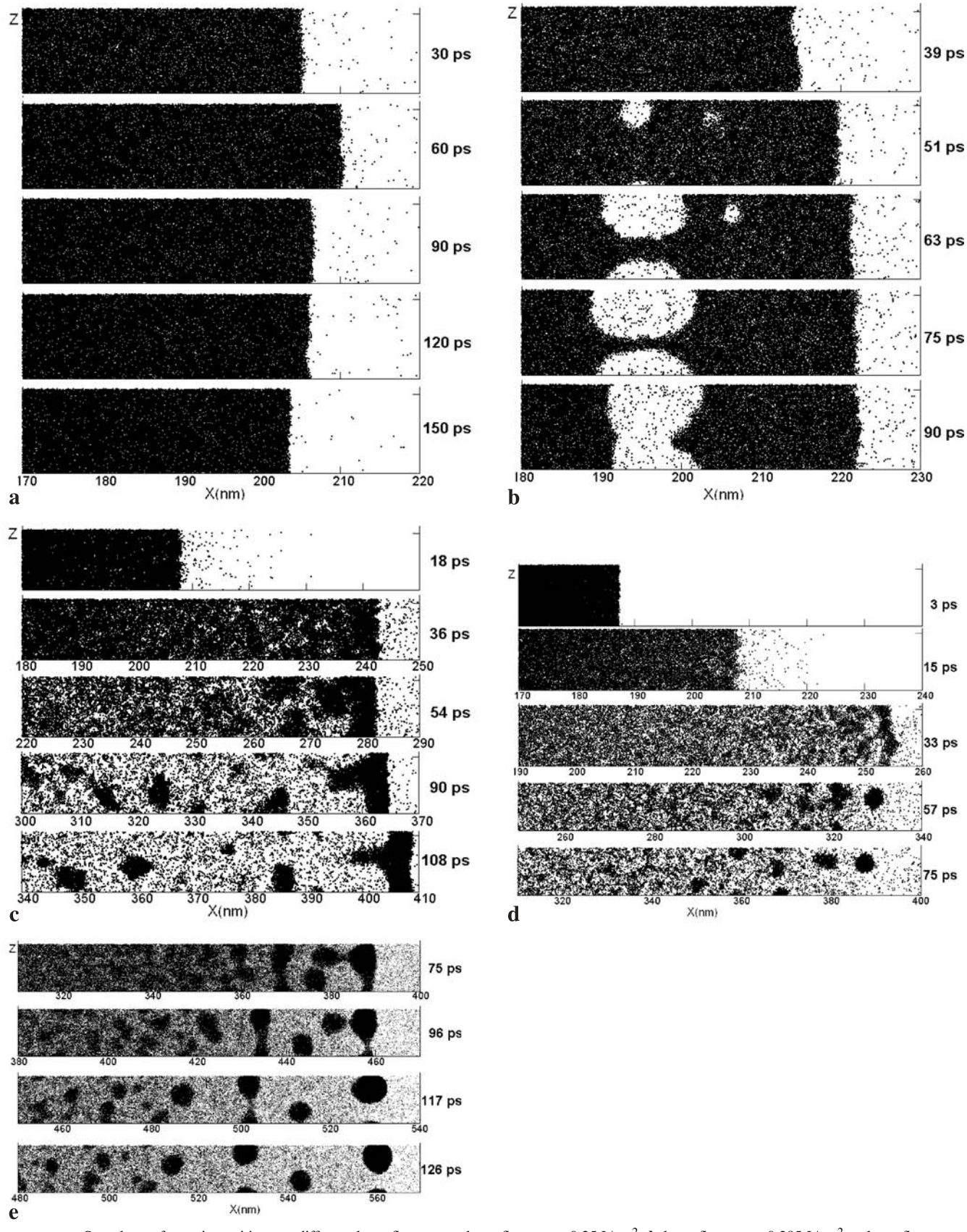

FIGURE 1 Snapshots of atomic positions at different laser fluences: **a** laser fluence = 0.25 J/cm^2, **b** laser fluence = 0.285 J/cm^2, **c** laser fluence = 0.65 J/cm^2, **d** laser fluence = 1.0 J/cm^2; 3 ps to 75 ps, **e** laser fluence = 1.0 J/cm^2; 75 ps to 126 ps

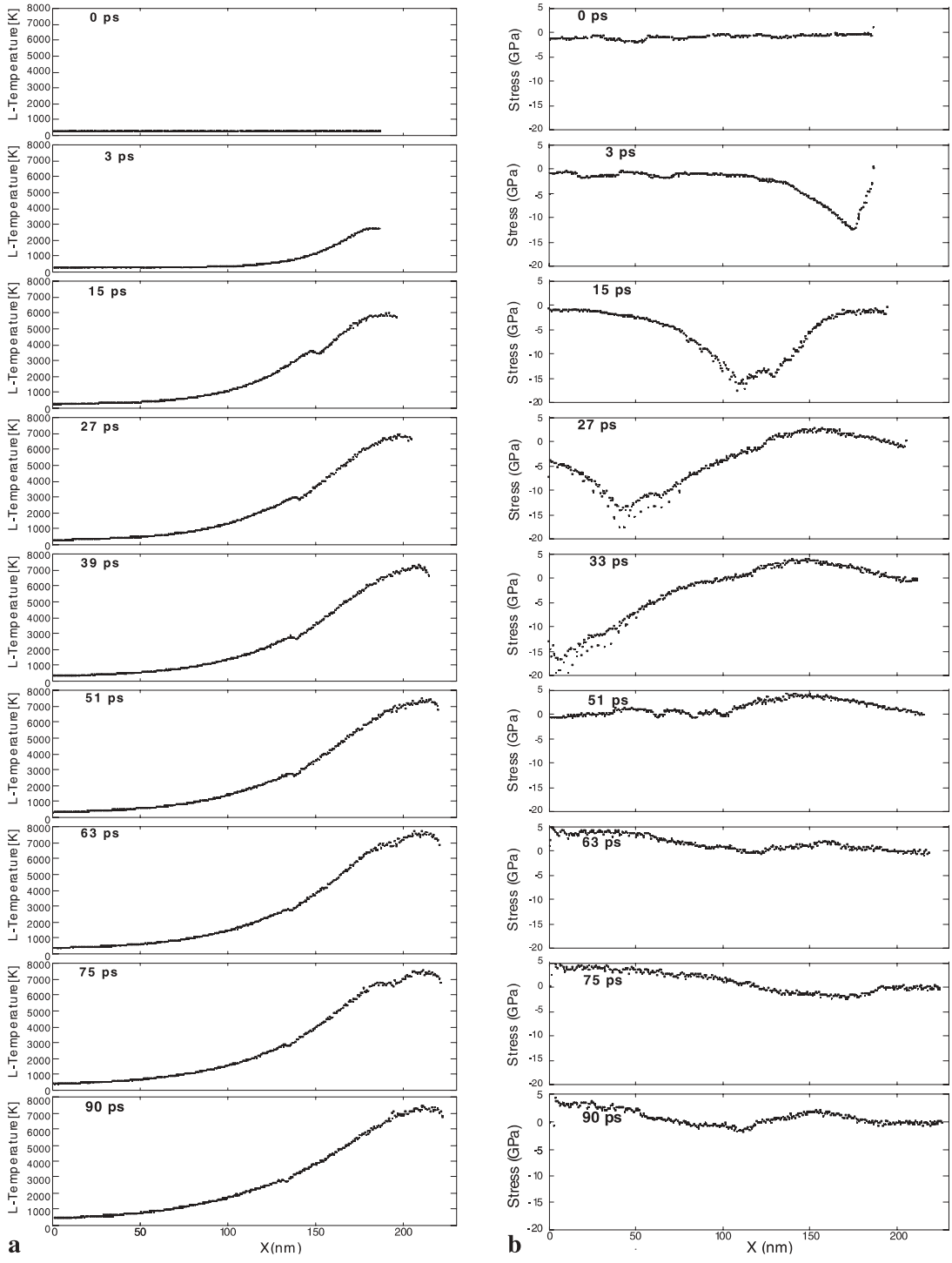

FIGURE 2 **a** Lattice temperature history and **b** stress wave at laser fluence of 0.285 J/cm^2

experimental value for nickel, 1728 K. Figure 2a shows that there is a temperature disorder after melting happens (for example, at about 150 nm at 15 ps). This disorder always occurs at the liquid–solid interface, therefore, it is due to the energy transfer associated with melting.

It is seen from Fig. 1b that gas bubbles are generated at 51 ps at about 195 nm (25 nm from the surface). These bubbles grow larger at later time steps and eventually break the domain into parts, which is considered as the origination of the volumetric type of material removal process.

Figure 2 reveals that gas bubbles appear at location where the tensile stress is very strong, but the lattice temperature is not necessarily the highest. For example, at 51 ps, a gas bubble appears at about 195 nm, while the highest lattice temperature is at around 210 nm, almost two times the absorption depth (8 nm) away. This is confirmed by the results of other laser fluences not presented here. This shows that the high lattice temperature is not the only reason for generating gas bubbles. The tensile stress can play an important role in the ablation process. On the other hand, it is noticed that the ten-

sile stress where the bubble starts to appear is not the highest. For this case (51 ps), the highest tensile stress is located at 140 nm, where the lattice temperature is only about 2900 K. This means that the tensile stress cannot generate gas bubbles at locations where the material is not hot enough. Therefore, it is concluded that the generation of the gas bubble is the combined results of both the high tensile stress and the high temperature. This is also found by other researchers [5], who consider the stress effect for void nucleation. The snapshots of atomic positions shown in that work are also similar to what we obtained here. A further analysis reveals that the lattice temperature needs to be higher than a certain value for the formation of gas bubbles. This threshold temperature is found to be about 7800 K from the results of this work, close to the critical temperature of nickel which is estimated to be 9400 ± 100 K from our calculation. It is known that when the temperature approaches the spinodal temperature (which is slightly lower than the critical temperature), a homogeneous nucleation called phase explosion occurs [19, 20]. However, it needs to be pointed out that the maximum temperature at higher laser fluences is found to exceed the critical temperature. This indicates that the mechanism for the generation and growth of the gas bubbles is different at high laser fluence. The thermodynamic and physical phenomena for high-fluence laser–material interaction is currently under investigation.

4 Conclusion

In this work, femtosecond laser ablation of nickel is studied using MD simulation. The detailed process of laser ablation is obtained, including the temperature history, generation and propagation of the stress wave, and bubble growth. A volumetric phase change process occurs, during which gas bubbles are formed inside the material. A threshold temperature is needed for the generation of gas bubbles, which is close to the thermodynamic critical temperature.

ACKNOWLEDGEMENTS Support to this work by the National Science Foundation (0219098-CTS) is greatly acknowledged. C. C. also thanks the Fellowship support from the Purdue Computational Research Institute.

REFERENCES

1 D. von der Linde, K. Sokolowski-Tinten: Appl. Surf. Sci. **154–155**, 1 (2000)
2 B.C. Stuart, M.D. Feit, S. Herman, A.M. Rubenchik, B.W. Shore, M.D. Perry: Phys. Rev. B **53**, 749 (1996)
3 W. Kautek, J. Krüger, M. Lenzner, S. Sartania, C. Spielmann, F. Krausz: Appl. Phys. Lett. **69**, 3146 (1996)
4 X. Wang, X. Xu: Int. J. Heat Mass Transf. **46**, 45 (2002)
5 L.V. Zhigilei, B.J. Garrison: J. Appl. Phys. **88**, 1281 (2000)
6 H.O. Jeschke, M.E. Garcia, K.H. Bennmann: Phys. Rev. Lett. **87**, 015 003 (2001)
7 S. Preuss, A. Demchuk, M. Stuke: Appl. Phys. A **61**, 33 (1995)
8 M.P. Allen, D.J. Tildesley: *Computer Simulation of Liquids* (Clarendon Press, Oxford 1987)
9 L.A. Girifalco, V.G. Weizer: Phys. Rev. **114**, 687 (1959)
10 X. Wang, X. Xu: Int. J. Heat Mass Transf. **46**, 45 (2002)
11 C. Schäfer, H.M. Urbassek, L.V. Zhigilei, B.J. Garrison: Comput. Mater. Sci. **24**, 421 (2002)
12 C. Cheng, X. Xu: Proceedings of 2003 ASME International Mechanical Engineering Congress and Exposition (IMECE'03), Washington, D.C., Nov. 16–21 (2003)
13 T.Q. Qiu, C.L. Tien: ASME J. Heat Transf. **115**, 835 (1993)
14 P.A. Atanasov, N.N. Nedialkov, S.E. Imamova, A. Ruf, H. Hügel, F. Dausinger, P. Berger: Appl. Surf. Sci. **186**, 369 (2002)
15 S. S Wellershoff, J. Hohlfeld, J. Güdde, E. Matthias: Appl. Phys. A **69**, S99 (1999)
16 R. Berman: *Thermal Conduction in Solids* (Clarendon Press, Oxford 1976)
17 J.M. Haile: *Molecular Dynamics Simulation: Elementary Methods* (John Wiley & Sons, New York 1992)
18 L.V. Zhigilei: Appli. Phys. A **76**, 339 (2003)
19 A. Miotello, R. Kelly: Appl. Phys. Lett. **67**, 3535 (1995)
20 K.H. Song, X. Xu: Appli. Surf. Sci. **127**, 111 (1998)